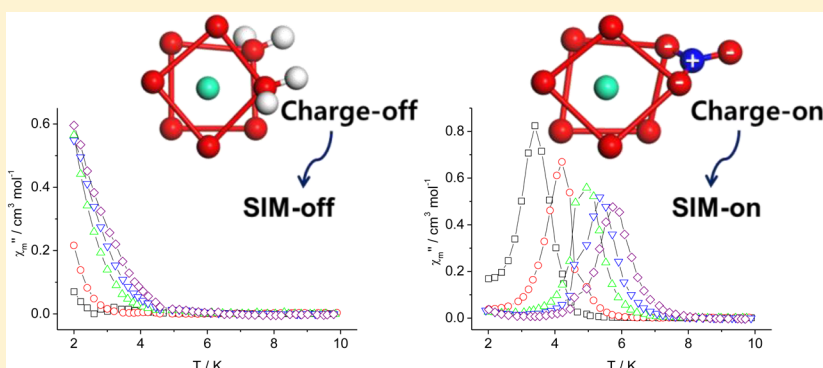


## Switching of Slow Magnetic Relaxation Dynamics in Mononuclear Dysprosium(III) Compounds with Charge Density

Kwang Soo Lim,<sup>†</sup> José J. Baldoví,<sup>‡</sup> Woo Ram Lee,<sup>†</sup> Jeong Hwa Song,<sup>†</sup> Sung Won Yoon,<sup>§</sup> Byoung Jin Suh,<sup>§</sup> Eugenio Coronado,<sup>‡</sup> Alejandro Gaita-Ariño,<sup>\*,‡</sup> and Chang Seop Hong<sup>\*,†</sup><sup>†</sup>Department of Chemistry, Korea University, Seoul 136-713, Republic of Korea<sup>‡</sup>Instituto de Ciencia Molecular (ICMol), Universidad de Valencia, C/Catedrático José Beltrán 2, E-46980 Paterna, Spain<sup>§</sup>Department of Physics, The Catholic University of Korea, Buchon 420-743, Republic of Korea

## Supporting Information



**ABSTRACT:** The symmetry around a Dy ion is recognized to be a crucial parameter dictating magnetization relaxation dynamics. We prepared two similar square-antiprismatic complexes,  $[\text{Dy}(\text{L}_{\text{OMe}})_2(\text{H}_2\text{O})_2](\text{PF}_6)$  (**1**) and  $\text{Dy}(\text{L}_{\text{OMe}})_2(\text{NO}_3)$  (**2**), where  $\text{L}_{\text{OMe}} = [\text{CpCo}\{\text{P}(\text{O})(\text{O}(\text{CH}_3)_2)_3\}]_3$ , including either two neutral water molecules (**1**) or an anionic nitrate ligand (**2**). We demonstrated that in this case relaxation dynamics is dramatically affected by the introduction of a charged ligand, stabilizing the easy axis of magnetization along the nitrate direction. We also showed that the application of either a direct-current field or chemical dilution effectively stops quantum tunneling in the ground state of **2**, thereby increasing the relaxation time by over 3 orders of magnitude at 3.5 K.

## INTRODUCTION

For more than 2 decades, single-molecule magnets (SMMs) have been a hot topic in molecular magnetism because of their rich physical behavior.<sup>1</sup> A breakthrough in the field was the discovery of slow relaxation of magnetization in a series of mononuclear *f*-element complexes coordinated by phthalocyaninato ligands in 2003.<sup>2–5</sup> This advance was consolidated a few years later with the report of a second family of mononuclear SMMs,<sup>6</sup> also known as single-ion magnets (SIMs). This dramatically increased the impact of this class of molecular nanomagnets, and since then, hundreds of analogues have been reported.<sup>7–12</sup>

From the point of view of molecular design, the power of these entities arises from the difference with the previous generation of SMMs, which was based on clusters of 3d transition-metal ions and where the properties depend on both the anisotropic properties of the individual metal ions and their exchange interactions. The magnetic and quantum properties of rare-earth SIMs can be modulated by playing with the ligand field around a single lanthanide ion, which means control of the properties is conceptually simpler in this second generation of SMMs.<sup>13–21</sup> Recent studies on SIMs with oblate 4f ions have

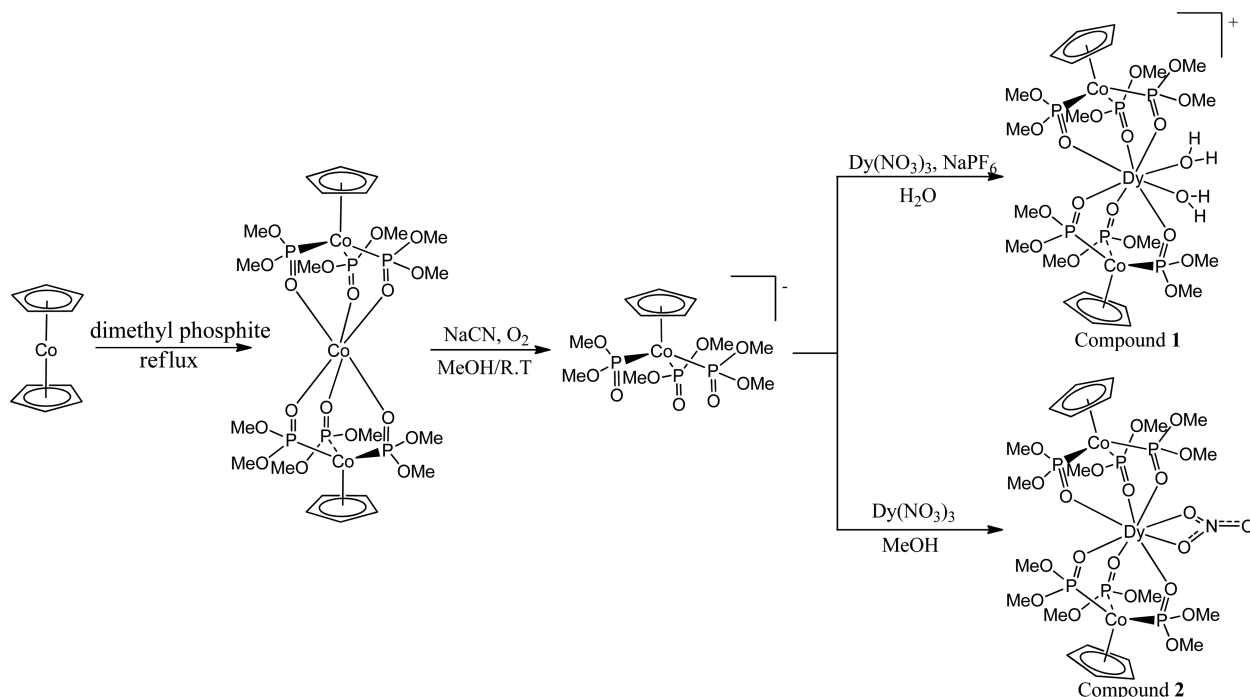
revealed that either weakening the electron density of the hard plane—e.g., by the attachment of electron-withdrawing groups or by the introduction of a weak-field ligand—or strengthening the electron density on the easy axis tends to increase the magnetic anisotropy, favoring high effective energy barriers.<sup>17,20,22–33</sup>

A general strategy to advance in the rational design of materials with improved properties is systematic study, in which a single parameter is changed. Applying this principle to the molecular design of SIMs, we decided to examine how the introduction of a charged ligand over one of the positions of the coordination sphere—maintaining a very similar coordination environment—controls the slow relaxation dynamics of the SIMs. Herein, we designed two compounds,  $[\text{Dy}(\text{L}_{\text{OMe}})_2(\text{H}_2\text{O})_2](\text{PF}_6)$  (**1**) and  $\text{Dy}(\text{L}_{\text{OMe}})_2(\text{NO}_3)$  (**2**), where  $\text{L}_{\text{OMe}} = [\text{CpCo}\{\text{P}(\text{O})(\text{O}(\text{CH}_3)_2)_3\}]_3$  (Scheme 1). In both examples, the Dy ions have near-identical square-antiprismatic geometries, except that two neutral water molecules coordinate to Dy in **1**, while the negatively charged nitrate ligand

Received: February 18, 2016

Published: May 17, 2016

Scheme 1. Synthetic Procedure for 1 and 2



coordinates to Dy in **2**. To the best of our knowledge, this straightforward strategy to characterize the magnetic effect of the ligand charge on a simple monomeric system has not been previously reported in the literature. Previous efforts in this direction include the study of the effect of an analogous series of  $\beta$ -diketone-based ligands,<sup>34,35</sup> which have slightly different charge densities but the same nominal charge, or the substitution of four water molecules by two nitrate anions and a methanol molecule, with a drastic change in the coordination geometry.<sup>36</sup>

## EXPERIMENTAL SECTION

**Reagents.** All chemicals and solvents in the synthesis were reagent-grade and used as received.  $\text{Na}[\text{CpCo}\{\text{P}(\text{O})(\text{OCH}_3)_2\}_3]$  ( $\text{NaL}_{\text{OMe}}$ ) was prepared according to literature procedures.<sup>37,38</sup>

$[\text{Dy}(\text{L}_{\text{OMe}})_2(\text{H}_2\text{O})_2](\text{PF}_6)$  (**1**). A mixture of  $\text{NaL}_{\text{OMe}}$  (48.9 mg, 0.10 mmol) and  $\text{NH}_4\text{PF}_6$  (16.3 mg, 0.10 mmol) was dissolved in water (15 mL) and stirred for 10 min. A yellow precipitate was generated as soon as an aqueous solution (2 mL) of  $\text{Dy}(\text{NO}_3)_3 \cdot 5\text{H}_2\text{O}$  (17.4 mg, 0.05 mmol) was added to the ligand solution. The mixture was stirred at room temperature for 12 h. The precipitate was filtered and washed with water. Yellow crystals formed after vapor diffusion of diethyl ether into a methanol solution of the crude product and were filtered off and dried in air. Yield: 68.4%. Anal. Calcd for  $\text{C}_{22}\text{H}_{50}\text{DyCo}_2\text{O}_{20}\text{F}_6\text{P}_7$ : C, 21.21; H, 4.05. Found: C, 21.14; H, 4.11.

$[\text{Y}(\text{L}_{\text{OMe}})_2(\text{H}_2\text{O})_2](\text{PF}_6)$  (**1-Y**). The Y analogue was obtained by the same procedure as that for compound **1**, except that  $\text{Y}(\text{NO}_3)_3 \cdot 6\text{H}_2\text{O}$  was used instead of  $\text{Dy}^{\text{III}}$ . Yield: 70.1%. Anal. Calcd for  $\text{C}_{22}\text{H}_{50}\text{YCo}_2\text{O}_{20}\text{F}_6\text{P}_7$ : C, 22.54; H, 4.30. Found: C, 22.79; H, 4.31.

$[\text{Y}_{0.98}\text{Dy}_{0.02}(\text{L}_{\text{OMe}})_2(\text{H}_2\text{O})_2](\text{PF}_6)$  (**diluted-1**). An aqueous solution (2 mL) of  $\text{Dy}(\text{NO}_3)_3 \cdot 5\text{H}_2\text{O}$  (0.001 mmol) and  $\text{Y}(\text{NO}_3)_3 \cdot 6\text{H}_2\text{O}$  (0.099 mmol) was added to a solution of  $\text{NaL}_{\text{OMe}}$  (0.20 mmol) and  $\text{NH}_4\text{PF}_6$  (0.20 mmol) in water (15 mL) with stirring. A yellow precipitate was generated and the mixture stirred at room temperature for 12 h. The precipitate was filtered, washed with water, and dried in air. Anal. Calcd for  $\text{C}_{22}\text{H}_{50}\text{Y}_{0.98}\text{Dy}_{0.02}\text{Co}_2\text{O}_{20}\text{F}_6\text{P}_7$ : C, 22.51; H, 4.29. Found: C, 22.87; H, 4.29.

$\text{Dy}(\text{L}_{\text{OMe}})_2(\text{NO}_3)$  (**2**). A mixture of  $\text{NaL}_{\text{OMe}}$  (48.9 mg, 0.10 mmol) and  $\text{Dy}(\text{NO}_3)_3 \cdot 5\text{H}_2\text{O}$  (17.4 mg, 0.05 mmol) was dissolved in

methanol (1.2 mL). The yellow solution was stirred at room temperature for 4 h and then filtered. Vapor diffusion of diethyl ether into a filtrate afforded yellow crystals. The product was washed with a small amount of cold methanol and water. Yield: 58.4%. Anal. Calcd for  $\text{C}_{22}\text{H}_{46}\text{Co}_2\text{DyO}_{21}\text{P}_6\text{N}$ : C, 23.45; H, 4.11; N, 1.24. Found: C, 23.17; H, 4.13; N, 1.19.

$\text{Y}(\text{L}_{\text{OMe}})_2(\text{NO}_3)$  (**2-Y**). The Y analogue was obtained by the same procedure as that for compound **2**, except that  $\text{Y}(\text{NO}_3)_3 \cdot 6\text{H}_2\text{O}$  was used instead of  $\text{Dy}^{\text{III}}$ . Yield: 49.3%. Anal. Calcd for  $\text{C}_{22}\text{H}_{46}\text{Co}_2\text{YO}_{21}\text{P}_6\text{N}$ : C, 25.09; H, 4.40; N, 1.33. Found: C, 24.81; H, 4.33; N, 1.21.

$\text{Y}_{0.96}\text{Dy}_{0.04}(\text{L}_{\text{OMe}})_2(\text{NO}_3)$  (**diluted-2**). A solution of  $\text{Dy}(\text{NO}_3)_3 \cdot 5\text{H}_2\text{O}$  (0.002 mmol) and  $\text{Y}(\text{NO}_3)_3 \cdot 6\text{H}_2\text{O}$  (0.098 mmol) in methanol (0.5 mL) was added to a solution of  $\text{NaL}_{\text{OMe}}$  (0.20 mmol) in methanol (0.7 mL) with stirring. The yellow solution was stirred for 4 h and then diffused with diethyl ether. The yellow powders that formed were filtered off and washed with cold methanol and water. Anal. Calcd for  $\text{C}_{22}\text{H}_{46}\text{Co}_2\text{Y}_{0.96}\text{Dy}_{0.04}\text{O}_{21}\text{P}_6\text{N}$ : C, 25.03; H, 4.39; N, 1.33. Found: C, 24.89; H, 4.30; N, 0.96.

**Physical Measurements.** Elemental analyses for C, H, and N were performed at the Elemental Analysis Service Center of Sogang University. IR spectra were obtained from powder samples with a Nicolet iS 10 spectrometer. Powder X-ray diffraction (PXRD) data were recorded using  $\text{Cu K}\alpha$  ( $\lambda = 1.5406 \text{ \AA}$ ) on a Rigaku Ultima III diffractometer with a scan speed of  $2^\circ \text{ min}^{-1}$  and a step size of  $0.02^\circ$ . Magnetic susceptibilities for complexes **1** and **2** were measured using a Quantum Design SQUID susceptometer (direct current, dc) and a PPMS magnetometer (alternating current, ac). Diamagnetic corrections of all samples were estimated from Pascal's Tables.

**Crystallographic Structure Determination.** X-ray data for **1**, **1-Y**, **2**, **2-Y**, **diluted-1**, and **diluted-2** were collected on a Bruker SMART APEXII diffractometer equipped with graphite-monochromated  $\text{Mo K}\alpha$  radiation ( $\lambda = 0.71073 \text{ \AA}$ ). Preliminary orientation matrix and cell parameters were determined from three sets of  $\phi$  scans at different starting angles. Data frames were obtained at scan intervals of  $0.5^\circ$  with an exposure time of  $10 \text{ s frame}^{-1}$ . The reflection data were corrected for Lorentz and polarization factors. Absorption corrections were carried out using *SADABS*. The structures were solved by direct methods and refined by full-matrix least-squares analysis using anisotropic thermal parameters for non-H atoms with the *SHELXTL*

program. Crystal data for **1**, **1-Y**, **2**, **2-Y**, diluted-**1**, and diluted-**2** are summarized in Table S1.

## RESULTS AND DISCUSSION

**Description of the Structures.** To obtain the targeted molecule, we reacted the tripodal ligand  $\{\text{CpCo}[\text{P}(\text{O})(\text{OMe})_2]_3\}^- [\text{L}_{\text{OMe}}^-]$  with  $\text{Dy}(\text{NO}_3)_3$  in the presence of  $\text{PF}_6^-$ , which served as the charge-balancing anion, to produce **1**. An identical procedure without using  $\text{PF}_6^-$  yielded compound **2**. **1** crystallizes in the orthorhombic  $P2_12_12$  space group, while **2** belongs to the monoclinic system with the  $P2_1/c$  space group. Each Dy center is octacoordinated by six O atoms from two  $\text{L}_{\text{OMe}}^-$  ligands and two O atoms from either two water molecules (**1**) or one nitrate anion (**2**), as shown in Figure 1.

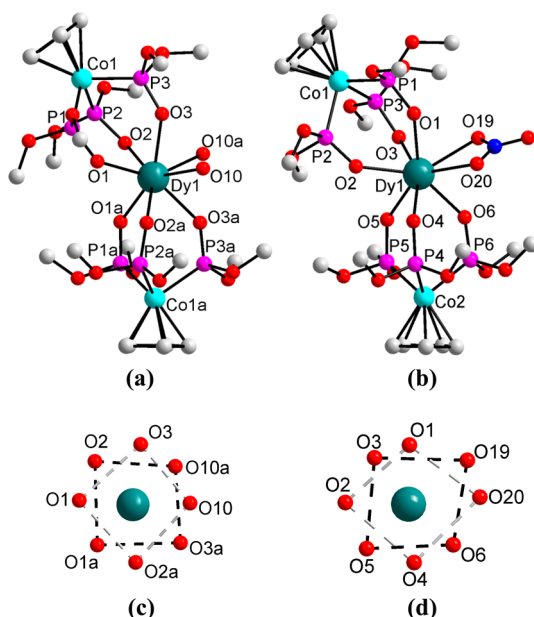


**Figure 1.** Molecular structures of (a) the cationic part of **1** and (b) **2**.  $D_{4d}$  coordination environment around Dy of (c) **1** and (d) **2**.

From the crystal structures, small but appreciable differences in the Dy–O bond lengths are observed from binding of the neutral ligands to Dy in **1** and that of the charged ligand to Dy in **2**: The Dy–O bond length ranges from 2.283(1) to 2.488(1) Å in **1** and from 2.289(1) to 2.508(1) Å in **2** (Table S2). To evaluate the exact geometry around the Dy ion, we carried out continuous-shape measure analysis.<sup>39</sup>  $S_X$ , which measures the normalized deviation from different ideal symmetries, showed that the geometries of both complexes lead to the local symmetry of  $\text{Dy}^{\text{III}}$  being close to square antiprism (SAPR), i.e.,  $D_{4d}$  (Table S3). The deviation is smaller in the case of **1**:  $S_{\text{SAPR}}(\mathbf{1}) = 0.829$ ;  $S_{\text{SAPR}}(\mathbf{2}) = 1.281$  (see Figures 1c,d). Such a more pronounced geometrical distortion in **2** arises from the chelation of  $\text{NO}_3^-$ , which results in a structural strain compared with two independent water molecules coordinating to Dy in **1**. The charge of  $[\text{Dy}(\text{L}_{\text{OMe}})_2(\text{H}_2\text{O})_2]^+$  is balanced in **1** by insertion of the  $\text{PF}_6^-$  counteranion in the crystal structure, whereas complex **2** is charge-neutral by itself. The existence of anions in **1** increases the Dy–Dy separation, with the shortest intermolecular Dy–Dy distances being 9.318(5) and 8.485(5) Å in **1** and **2**, respectively.

**Magnetic Properties.** The dc magnetic susceptibilities ( $\chi_{\text{m}}T$ ) of **1** and **2** were measured in the temperature range of

2–300 K at 1000 G (Figure 2). The  $\chi_{\text{m}}T$  values of **1** and **2** at room temperature are close to the theoretical value of 14.17

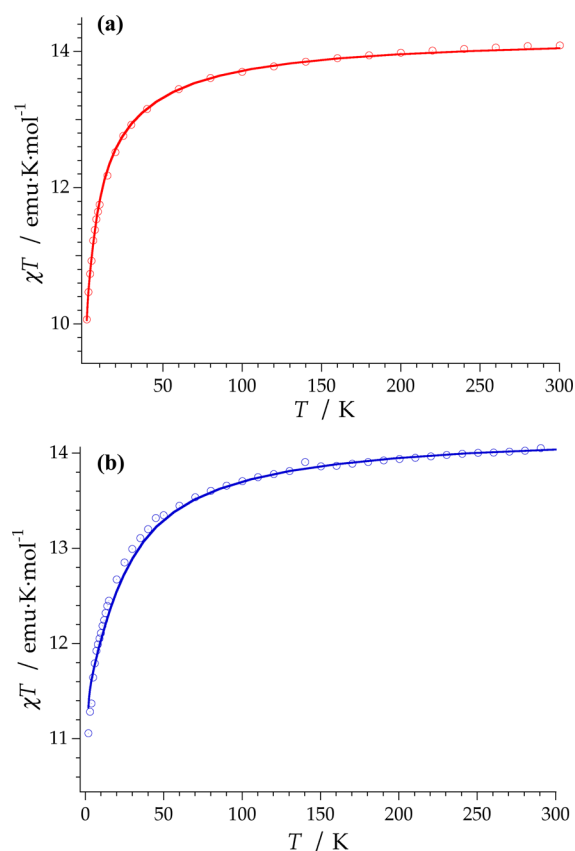


**Figure 2.** Fitting of the experimental  $\chi T$  products of **1** (a) and **2** (b) from 2 to 300 K using the REC model in the SIMPRE package (solid line).

$\text{cm}^3 \text{K mol}^{-1}$  predicted for one  $\text{Dy}^{\text{III}}$  ion ( ${}^6\text{H}_{15/2}$ ,  $S = 5/2$ ,  $L = 5$ , and  $g = 4/3$ ). Upon cooling, the  $\chi_{\text{m}}T$  curve first decreases gradually and then decreases more rapidly below 50 K, which is attributed to thermal depopulation of the Stark sublevels. As shown in the  $M$  versus  $H/T$  plot (Figures S2 and S3), below 6 K magnetization linearly increases at low fields for both compounds. Compound **1** does not reach saturation even at 2 K and 7 T and presents  $M$  versus  $H/T$  curves at different temperatures, which are displaced from each other, pointing toward the population of energy levels at these temperatures. In contrast, magnetization of compound **2** reaches a saturation value of approximately 5.5  $N\beta$  at around 5000 G/K and presents  $M$  versus  $H/T$  curves at different temperatures, which are superimposed with each other, as could be expected for an isolated Ising spin.

The dynamic magnetic properties were examined by ac magnetic susceptibility measurements using an ac field of 4 G at several oscillating frequencies. The temperature-dependent ac data of **1** were obtained at zero field under an external field  $H_{\text{dc}} = 1000$  G, and no peaks were found (Figure S4). When the dependence of the out-of-phase ac susceptibility of **1** was studied at increasing fields from 0 to 1200 G, the same behavior was observed (Figure S5). On the other hand, the dynamic magnetic properties of **2** displayed in Figure 3a,b show that, below 8.0 K, the  $\chi_{\text{m}}''$  peaks vary with respect to the oscillating frequency, indicating slow magnetic relaxation. The slow spin dynamics in **2** is also corroborated by the frequency-dependent

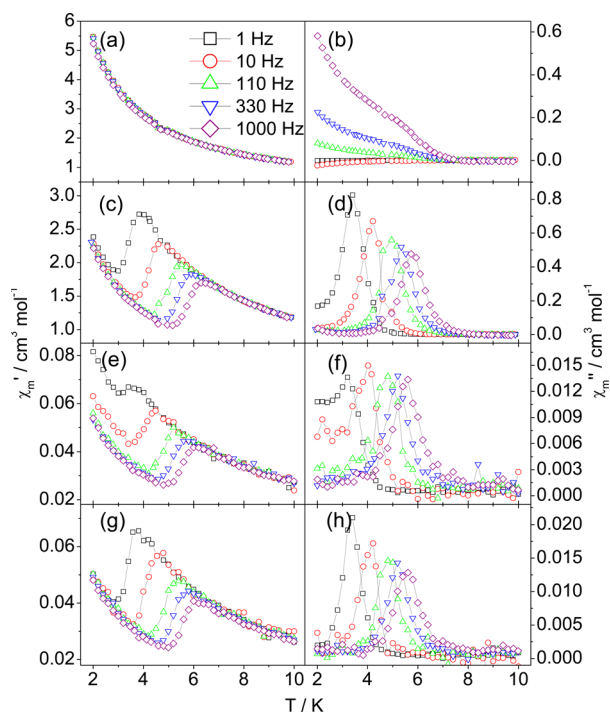


**Figure 3.** Temperature dependence of in-phase ( $\chi_m'$ ) and out-of-phase ( $\chi_m''$ ) ac susceptibilities at  $H_{dc} = 0$  (a and b) and 1.0 kG (c and d) for **2** and at  $H_{dc} = 0$  (e and f) and 1.0 kG (g and h) for diluted-**2**.

ac data collected at  $T = 2-8$  K (Figure S6). The  $\ln(\tau)$  versus  $1/T$  plot for **2** presents some curvature (Figure 4), indicating that

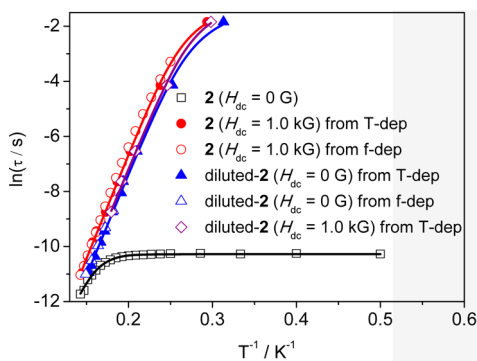


**Figure 4.** Arrhenius plots of relaxation time data for **2** and diluted-**2**.

the dynamics cannot be properly modeled assuming a simple Orbach mechanism. The data could be fitted considering temperature-independent quantum tunneling ( $\tau_{QTM}$ ) and thermally activated Orbach [ $\propto \exp(-U_{eff}/kT)$ ] and Raman processes ( $\propto T^n$ ), using the following equation:<sup>23,40,41</sup>

$$\tau^{-1} = \tau_{QTM}^{-1} + CT^n + \tau_0^{-1} \exp(-U_{eff}/kT) \quad (1)$$

where  $\tau$  is the inverse of the ac frequency,  $T$  is the temperature of the maximum in the ac signal,  $U_{eff}$  is the effective energy barrier,  $k$  is Boltzmann's constant, and  $\tau_{QTM}$ ,  $C$ , and  $\tau_0$  are the fitting parameters of the different relaxation mechanisms. The fit in the temperature range  $T = 2-7$  K resulted in  $\tau_{QTM} = 3.44 \times 10^{-5}$  s,  $n = 5$ ,  $C = 0.04547$  s<sup>-1</sup> K<sup>-5</sup>,  $\tau_0 = 2.92 \times 10^{-10}$  s, and an effective energy barrier of  $U_{eff} = 51.2$  cm<sup>-1</sup> (Figure 4). These results corroborate that, in addition to quantum tunneling and Orbach pathways, Raman relaxation is operative in **2**. The

Cole–Cole plots at a temperature range of 2–8 K give  $\alpha$  parameters of less than 0.28 (Figure S7), possibly because of two very close relaxation processes, as can be seen in Figure S7 with a nonsymmetric semicircle. To reduce the quantum tunneling effect, we inspected the field-dependent relaxation time at  $T = 5$  K and determined the optimal field to be 1.0 kG (Figures S8 and S9): under this external field, **2** presents prominent slow relaxation (Figures 3c,d and S10). Both  $\chi_m'$  and  $\chi_m''$  susceptibilities exhibit significant frequency-dependent peaks between 4 and 7 K (Figure S11). The Arrhenius plot unveils complete suppression of the quantum tunneling under 1.0 kG in **2**. This fit was carried out taking into account the Raman term ( $C$ ) in eq 1, resulting in  $n = 5$ ,  $C = 0.01071$  s<sup>-1</sup> K<sup>-5</sup>,  $\tau_0 = 3.14 \times 10^{-10}$  s, and  $U_{eff} = 53.0$  cm<sup>-1</sup>. Thus, the behavior at low temperature, which deviates from linearity, is attributed to Raman relaxation. The Cole–Cole plot results in  $\alpha < 0.1$ , a smaller value compared with **2** without the applied external field (Figure S12), indicating a lesser importance of secondary relaxation processes.

It is striking that, although the central geometry around Dy in **2** is more distorted than that in **1**, SMM characteristics are only evident in **2**. This is in contrast to simple symmetry considerations: intuitively, a coordination environment that is close to square-antiprismatic (i.e., near perfect  $D_{4d}$ ) results in pure  $M_J$  quantization, which means no avoided crossings, and if one assumes a Landau–Zener mechanism, this means the tunneling probability would fall to zero. The present experimental observation shows that the mere substitution of one ligand for another with a different effective charge dramatically affects the magnetic dynamics. This notable feature can be mainly ascribed to the dominant charge effect of ligand coordination on the relaxation dynamics over symmetry considerations, switching the SMM behavior on or off. In fact, in heteroleptic complexes, such as the present case, the different charges carried by the different ligands need to be taken into account and complicate purely symmetry-based arguments because the real symmetry is much lower than the apparent one.

To complete our understanding of these systems, it is essential to study the effect of the magnetic dipolar interaction on quantum tunneling.<sup>42</sup> For this purpose, we treated Y<sup>3+</sup> instead of Dy<sup>3+</sup> with NaL<sub>OMe</sub> under the same experimental conditions: Y-containing products **1-Y** and **2-Y** were successfully isolated (Figures S13 and S14). The Dy-containing samples were magnetically diluted following the reaction procedure and partial replacement of Dy in **1** (or **2**) with diamagnetic Y<sup>3+</sup> ions. As shown by the PXRD data in Figures S15 and S16, the profiles of the diluted samples are consistent with the simulated pattern, suggesting that they are isostructural. Elemental and inductively coupled plasma analyses demonstrate that the average ratio of Dy/Y in diluted-**1** and diluted-**2** corresponds to 0.98:0.02 and 0.96:0.04, respectively. The crystal structures of the diluted samples were determined; the Y–O and (Y, Dy)–O bond lengths range from 2.268(10) to 2.477(12) Å in **1-Y**, from 2.263(1) to 2.493(1) Å in **2-Y**, from 2.265(2) to 2.459(3) Å in diluted-**1**, and from 2.271(1) to 2.496(1) Å in diluted-**2** (Figures S17 and S18). Compared with **1** and **2**, the square-antiprismatic geometry around the central metal ion in each diluted compound is more distorted; this might be due to either the inhomogeneity of the metal composition or the slightly different radius of the Y<sup>3+</sup> cation (Table S3).

It is a fact that, in the diluted samples of both **1** and **2**, a diamagnetic Y matrix is doped with 2% and 4% of Dy, respectively, achieving a sufficient separation between neighboring Dy atoms so that the dipolar interaction between them can be neglected. In **1**, this has no effect: the peak in  $\chi_m''$  was not observed in diluted-**1** even under an external magnetic field (Figure S3e–h). In contrast, for diluted-**2** (Figures 3e,f and S19 and S20), the maximum in  $\chi_m''$  varies with the frequency, which is characteristic of slow magnetic relaxation in SMMs. As shown in Figure S21, the narrow distribution ( $\alpha < 0.11$ ) of single relaxation processes is observed from the Cole–Cole plots, and the Arrhenius plot reveals  $n = 5$ ,  $C = 0.01647 \text{ s}^{-1} \text{ K}^{-5}$ ,  $\tau_0 = 2.35 \times 10^{-10} \text{ s}$ , and  $U_{\text{eff}} = 51.5 \text{ cm}^{-1}$  (Figure 4). The application of a magnetic field of 1.0 kG affords  $n = 5$ ,  $C = 0.01098 \text{ s}^{-1} \text{ K}^{-5}$ ,  $\tau_0 = 2.81 \times 10^{-10} \text{ s}$ , and  $U_{\text{eff}} = 51.5 \text{ cm}^{-1}$ , which are very close to the values without a field.

These results verify that either the application of a dc field or the suppression of Dy–Dy dipolar interactions upon magnetic dilution can effectively stop quantum tunneling in the ground state, thereby increasing the relaxation time notably by over 3 orders of magnitude at a given temperature (3.5 K). Remarkably, these two radically different methods to solve the same problem result in virtually the same final properties, as can be observed by the almost-overlapping data in Figure 4.

**Theoretical Calculations.** To explain the differences in the magnetic behavior of both derivatives, we have used the radial effective charge (REC) model,<sup>43</sup> introducing the crystal structures of **1** and **2** as input in the *SIMPRES* computational package.<sup>44,45</sup> For this purpose, we require two parameters ( $D_r$  and  $Z_i$ ) for each kind of ligand ( $L_{\text{OMe}}$ ,  $\text{H}_2\text{O}$ , and  $\text{NO}_3^-$ ). Such parameters are obtained from a fit of the magnetic properties of each complex (for further information, see the Supporting Information, pp S23–S27). In the case of the O atoms from the water molecules and the  $\text{NO}_3^-$  anion, the REC parameters utilized from a recent study,<sup>46</sup> in which a series of polyoxometalate-based lanthanide complexes were modeled, are introduced as starting values. When this procedure is employed, an excellent fit of the  $\chi_m T$  powder data is obtained with the following parameters for each coordinated O atom in the  $L_{\text{OMe}}$  ligand ( $D_r = 0.42 \text{ \AA}$  and  $Z_i = 0.84$ ), O atoms of the water molecules ( $D_r = 0.78 \text{ \AA}$  and  $Z_i = 0.46$ ), and each of the two O atoms involved in the coordination by the  $\text{NO}_3^-$  anion ( $D_r = 0.813 \text{ \AA}$  and  $Z_i = 0.31$ ) (Figure 2). Here one needs to recall that these are effective charges and distances used by *SIMPRES* to predict the spin-energy levels and wave functions and are not an attempt to simulate an actual charge distribution.

According to our calculations, the difference between the energy levels of both compounds is remarkable (Figure S22), and this explains why slow relaxation of magnetization is obtained only in **2**. In **1** ( $g_z = 14.3$ ), we have found a ground state with a wave function described by 69% of  $\pm^{13}/_2$  and 17% of  $\pm^7/_2$ , with the first excited state located at  $1 \text{ cm}^{-1}$  with a wave function described by 35% of  $\pm^{15}/_2$ , 27% of  $\pm^{11}/_2$ , 10% of  $\pm^9/_2$ , and 10% of  $\mp^7/_2$ . This energy difference is below the precision of *SIMPRES*, or indeed of any existing theoretical method used to determine the spin-energy levels in lanthanide complexes. Additionally, one should expect slight distortions in the coordination environment due to (1) the flexibility of the water molecules and (2) thermal effects: ac measurements are performed at low temperature (between 2 and 10 K), whereas the structures used as input are measured at room temperature (296 K). Note that thermal variations on the order of  $5 \text{ cm}^{-1}$  between the ground and first excited states have been reported

using both ab initio and effective electrostatic methods.<sup>47</sup> This, together with the absence of SMM behavior in **1**, allows us to say that a thermal mechanism via a very low-lying level can still be active at 2 K, but we are unable to unequivocally determine the nature of the ground state in **1**. In contrast, in **2**, the ground-state function is calculated to be 90% of  $\pm^{15}/_2$  ( $g_z = 18.8$ ) and the first excited state is located at approximately  $42 \text{ cm}^{-1}$ , which is similar to the energy barrier experimentally determined in diluted-**2**. This is evidence that the ground state of **2** has an almost Ising character and is well isolated from excited states, allowing the observed slow relaxation of magnetization.

Regarding the calculation of the magnetic anisotropy via effective electrostatic models, one needs to note that this approach has only been used in the past in cases with particularly simple environments.<sup>48</sup> This is mainly due to the fact that the REC model only considers the first coordination sphere and was originally designed to calculate the spin-energy levels and wave functions. In this case, the ligands include a high number of charges beyond the coordination sphere, something that can induce drastic changes in the magnetic anisotropy.<sup>12</sup> In this context, an interesting approach that takes into account the entire molecule using an electrostatic minimization strategy from formal charges is the *MAGELLAN* software package.<sup>17,23</sup> The application of the program to **2** results in a preferred magnetic anisotropy axis that is not parallel to the near- $C_4$  axis, in sharp contrast with the behavior observed in square-antiprismatic SIMs (Figure 5). Indeed, the

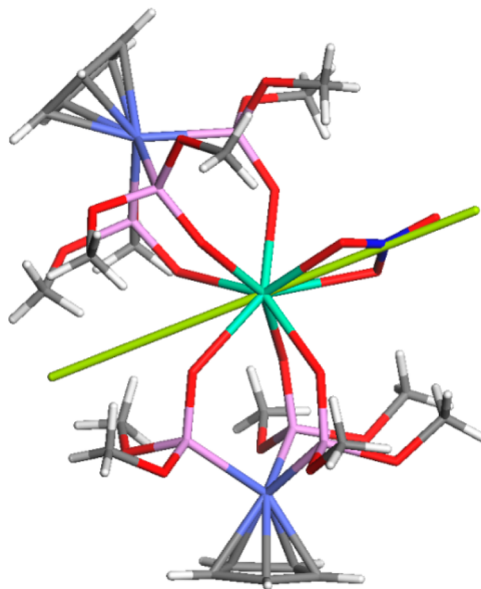


**Figure 5.** Orientation of the anisotropy axis of **2** according to the *MAGELLAN* software package.

enhancement in the charge density by the nitrate ligand in **2**, compared with that of the neutral water ligands in **1**, forces the magnetic easy axis to be oriented along the nitrate direction, eventually stabilizing the oblate electron density of the Dy ion. Although it is possible that minor ligand-field differences of the ligands or slight differences in the coordination geometry can have an effect on the magnetic anisotropy, this finding demonstrates that an efficient approach to generating strong magnetic anisotropy is a direct introduction of a charged ligand to a system of interest.

## CONCLUSIONS

We have prepared and characterized two dysprosium(III) complexes coordinated by neutral water molecules (1) or a nitrate anion (2). Notably, in this system, the relaxation dynamics are dominated not by the central symmetry around Dy but by the charge density in the nitrate/water coordinating position. As is general in science, systematic studies in which a single parameter is changed are the way to advance in the rational design of materials with improved properties. In the present example, we have shown the key role played by the presence of a charged ligand in a square-antiprismatic dysprosium complex to tune its magnetic and quantum properties. Furthermore, we have shown that two independent strategies, namely, the application of an optimal external field or a magnetic dilution, lead to the suppression of quantum tunneling and thus slow magnetic relaxation by 3 orders of magnitude.

## ASSOCIATED CONTENT

### Supporting Information

The Supporting Information is available free of charge on the ACS Publications website at DOI: 10.1021/acs.inorgchem.6b00410.

12 tables, 23 figures, and additional content (PDF)

X-ray crystallographic data in CIF format (CIF)

## AUTHOR INFORMATION

### Corresponding Authors

\*E-mail: alejandro.gaita@uv.es.

\*E-mail: cshong@korea.ac.kr.

### Notes

The authors declare no competing financial interest.

## ACKNOWLEDGMENTS

This work was supported by the Korea CCS R&D Center funded by the Korea government (The Ministry of Science, ICT & Future Planning; Grant NRF-2014M1A8A1049253), by Basic Science Research Program (Grant NRF-2015R1A2A1A10055658), and by Priority Research Centers Program (Grant NRF20120005860). W.R.L. was partly supported by a Korea University grant. We also thank the EU (ERC Advanced Grant SPINMOL and ERC Consolidator Grant DECRESIM), the Spanish MINECO (Grants MAT2014-56143-R, CTQ2014-52758-P, and "Unidad de Excelencia María de Maeztu" MDM-2015-0538 granted to ICMol), and the Generalitat Valenciana (Prometeo and ISIC Programmes of excellence). A.G.-A. acknowledges funding by the MINECO (Ramón y Cajal contract).

## REFERENCES

- (1) Winpenny, R. *Single-Molecule Magnets and Related Phenomena; Structure and Bonding Series 122*; Springer-Verlag: Berlin, 2006.
- (2) Ishikawa, N.; Sugita, M.; Ishikawa, N.; Koshihara, S.-y.; Kaizu, Y. *J. Phys. Chem. B* **2004**, *108*, 11265–11271.
- (3) Ishikawa, N.; Sugita, M.; Ishikawa, N.; Koshihara, S.-y.; Kaizu, Y. *J. Am. Chem. Soc.* **2003**, *125*, 8694–8695.
- (4) Ishikawa, N.; Mizuno, Y.; Takamatsu, S.; Ishikawa, T.; Koshihara, S.-y. *Inorg. Chem.* **2008**, *47*, 10217–10219.
- (5) Ishikawa, N.; Sugita, M.; Wernsdorfer, W. *J. Am. Chem. Soc.* **2005**, *127*, 3650–3651.
- (6) Aldamen, M. A.; Clemente-Juan, J. M.; Coronado, E.; Martí-Gastaldo, C.; Gaita-Ariño, A. *J. Am. Chem. Soc.* **2008**, *130*, 8874–8875.

- (7) Woodruff, D. N.; Winpenny, R. E.; Layfield, R. A. *Chem. Rev.* **2013**, *113*, 5110–5148.
- (8) Sorace, L.; Benelli, C.; Gatteschi, D. *Chem. Soc. Rev.* **2011**, *40*, 3092–3104.
- (9) Jia, L.; Chen, Q.; Meng, Y.-S.; Sun, H.-L.; Gao, S. *Chem. Commun.* **2014**, *50*, 6052–6055.
- (10) Yin, D.-D.; Chen, Q.; Meng, Y.-S.; Sun, H.-L.; Zhang, Y.-Q.; Gao, S. *Chem. Sci.* **2015**, *6*, 3095–3101.
- (11) Shang, H.; Zeng, S.; Wang, H.; Dou, J.; Jiang, J. *Sci. Rep.* **2015**, *5*, 8838.
- (12) Cucinotta, G.; Perfetti, M.; Luzon, J.; Etienne, M.; Car, P. E.; Caneschi, A.; Calvez, G.; Bernot, K.; Sessoli, R. *Angew. Chem., Int. Ed.* **2012**, *51*, 1606–1610.
- (13) Rinehart, J. D.; Fang, M.; Evans, W. J.; Long, J. R. *Nat. Chem.* **2011**, *3*, 538–542.
- (14) Rinehart, J. D.; Fang, M.; Evans, W. J.; Long, J. R. *J. Am. Chem. Soc.* **2011**, *133*, 14236–14239.
- (15) Demir, S.; Jeon, I.-R.; Long, J. R.; Harris, T. D. *Coord. Chem. Rev.* **2015**, *289–290*, 149–176.
- (16) Aravena, D.; Ruiz, E. *Inorg. Chem.* **2013**, *52*, 13770–13778.
- (17) Chilton, N. F.; Collison, D.; McInnes, E. J.; Winpenny, R. E.; Soncini, A. *Nat. Commun.* **2013**, *4*, 2551–2557.
- (18) Ungur, L.; Le Roy, J. J.; Korobkov, I.; Murugesu, M.; Chibotaru, L. F. *Angew. Chem., Int. Ed.* **2014**, *53*, 4413–4417.
- (19) Coutinho, J. T.; Antunes, M. A.; Pereira, L. C. J.; Marçalo, J.; Almeida, M. *Chem. Commun.* **2014**, *50*, 10262–10264.
- (20) Rinehart, J. D.; Long, J. R. *Chem. Sci.* **2011**, *2*, 2078–2085.
- (21) Lin, S. Y.; Guo, Y. N.; Guo, Y.; Zhao, L.; Zhang, P.; Ke, H.; Tang, J. *Chem. Commun.* **2012**, *48*, 6924–6926.
- (22) Tuna, F.; Smith, C. A.; Bodensteiner, M.; Ungur, L.; Chibotaru, L. F.; McInnes, E. J.; Winpenny, R. E.; Collison, D.; Layfield, R. A. *Angew. Chem., Int. Ed.* **2012**, *51*, 6976–6980.
- (23) Demir, S.; Zadrozny, J. M.; Long, J. R. *Chem. - Eur. J.* **2014**, *20*, 9524–9529.
- (24) Habib, F.; Brunet, G.; Vieru, V.; Korobkov, I.; Chibotaru, L. F.; Murugesu, M. *J. Am. Chem. Soc.* **2013**, *135*, 13242–13245.
- (25) Chilton, N. F.; Goodwin, C. A. P.; Mills, D. P.; Winpenny, R. E. *P. Chem. Commun.* **2015**, *51*, 101–103.
- (26) Chilton, N. F. *Inorg. Chem.* **2015**, *54*, 2097–2099.
- (27) Gregson, M.; Chilton, N. F.; Ariciu, A.-M.; Tuna, F.; Crowe, I. F.; Lewis, W.; Blake, A. J.; Collison, D.; McInnes, E. J. L.; Winpenny, R. E. P.; Liddle, S. T. *Chem. Sci.* **2016**, *7*, 155–165.
- (28) Li, X. L.; Li, H.; Chen, D. M.; Wang, C.; Wu, J.; Tang, J.; Shi, W.; Cheng, P. *Dalton Trans.* **2015**, *44*, 20316–20320.
- (29) Sun, W.-B.; Yan, P.-F.; Jiang, S.-D.; Wang, B.-W.; Zhang, Y.-Q.; Li, H.-F.; Chen, P.; Wang, Z.-M.; Gao, S. *Chem. Sci.* **2016**, *7*, 684–691.
- (30) Pugh, T.; Tuna, F.; Ungur, L.; Collison, D.; McInnes, E. J.; Chibotaru, L. F.; Layfield, R. A. *Nat. Commun.* **2015**, *6*, 7492.
- (31) Brunet, G.; Habib, F.; Korobkov, I.; Murugesu, M. *Inorg. Chem.* **2015**, *54*, 6195–6202.
- (32) Cao, W.; Gao, C.; Zhang, Y.-Q.; Qi, D.; Liu, T.; Wang, K.; Duan, C.; Gao, S.; Jiang, J. *Chem. Sci.* **2015**, *6*, 5947–5954.
- (33) Pugh, T.; Vieru, V.; Chibotaru, L. F.; Layfield, R. A. *Chem. Sci.* **2016**, *7*, 2128–2137.
- (34) Chen, G.-J.; Guo, Y.-N.; Tian, J.-L.; Tang, J.; Gu, W.; Liu, X.; Yan, S.-P.; Cheng, P.; Liao, D.-Z. *Chem. - Eur. J.* **2012**, *18*, 2484–2487.
- (35) Bi, Y.; Guo, Y.-N.; Zhao, L.; Guo, Y.; Lin, S.-Y.; Jiang, S.-D.; Tang, J.; Wang, B.-W.; Gao, S. *Chem. - Eur. J.* **2011**, *17*, 12476–12481.
- (36) Chilton, N. F.; Langlely, S. K.; Moubaraki, B.; Soncini, A.; Batten, S. R.; Murray, K. S. *Chem. Sci.* **2013**, *4*, 1719–1730.
- (37) Klaui, W.; Eberspach, W.; Gütllich, P. *Inorg. Chem.* **1987**, *26*, 3977–3982.
- (38) Klaui, W.; Eberspach, W.; Schwarz, R. *J. Organomet. Chem.* **1983**, *252*, 347–357.
- (39) Álvarez, S.; Alemany, P.; Casanova, D.; Cirera, J.; Llunell, M.; Avnir, D. *Coord. Chem. Rev.* **2005**, *249*, 1693–1708.
- (40) Brown, A. J.; Pinkowicz, D.; Saber, M. R.; Dunbar, K. R. *Angew. Chem., Int. Ed.* **2015**, *54*, 5864–5868.

- (41) Meihaus, K. R.; Minasian, S. G.; Lukens, W. W., Jr.; Kozimor, S. A.; Shuh, D. K.; Tyliszczak, T.; Long, J. R. *J. Am. Chem. Soc.* **2014**, *136*, 6056–6068.
- (42) Habib, F.; Lin, P. H.; Long, J.; Korobkov, I.; Wernsdorfer, W.; Murugesu, M. *J. Am. Chem. Soc.* **2011**, *133*, 8830–8833.
- (43) Baldoví, J. J.; Borrás-Almenar, J. J.; Clemente-Juan, J. M.; Coronado, E.; Gaita-Ariño, A. *Dalton Trans.* **2012**, *41*, 13705–13710.
- (44) Baldoví, J. J.; Cardona-Serra, S.; Clemente-Juan, J. M.; Coronado, E.; Gaita-Ariño, A.; Pali, A. *J. Comput. Chem.* **2013**, *34*, 1961–1967.
- (45) Baldoví, J. J.; Clemente-Juan, J. M.; Coronado, E.; Gaita-Ariño, A.; Pali, A. *J. Comput. Chem.* **2014**, *35*, 1930–1934.
- (46) Baldoví, J. J.; Clemente-Juan, J. M.; Coronado, E.; Duan, Y.; Gaita-Ariño, A.; Giménez-Saiz, C. *Inorg. Chem.* **2014**, *53*, 9976–9980.
- (47) Qian, K.; Baldoví, J. J.; Jiang, S.-D.; Gaita-Ariño, A.; Zhang, Y.-Q.; Overgaard, J.; Wang, B.-W.; Coronado, E.; Gao, S. *Chem. Sci.* **2015**, *6*, 4587–4593.
- (48) Baldoví, J. J.; Clemente-Juan, J. M.; Coronado, E.; Gaita-Ariño, A. *Inorg. Chem.* **2014**, *53*, 11323–11327.